Interplay of charge exchange and energy loss of 0.67–1.5-MeV He ions specularly reflected from a crystal surface

Yoshikazu Fujii, Shinsuke Fujiwara, Kazumasa Narumi, Kenji Kimura, and Michi-hiko Mannami
Department of Engineering Science, Kyoto University, Kyoto 606-01, Japan
(Received 6 July 1993; revised manuscript received 27 October 1993)

Charge-state distributions and energy losses of 0.67–1.5-MeV He ions scattered from a clean (100) surface of a SnTe single crystal are studied at glancing-angle incidence under UHV conditions. A stochastic model of charge exchange and energy loss of ions is developed, where inelastic interactions depend on the distance of the ion from the surface. Observed charge-state fractions and energy losses of the reflected He ions are explained with the model. Taking account of scattering of ions at surface steps, which causes the deflection of ion trajectories, position-dependent charge-exchange probabilities of He ions near the surface are derived from the observed charge-state distributions and charge-state dependence of the energy losses of scattered He ions.

PACS number(s): 34.50.Bw, 34.70.+e, 79.20.Rf, 61.80.Mk

I. INTRODUCTION

Fast ions incident on an atomically flat crystal surface interact only with atoms on the topmost atomic plane of the surface when the angle of incidence θ_i is small. Their trajectories are described approximately by the equation of motion of the ion in a continuum planar potential due to the surface atoms as in the case of planar channeling of fast ions [1,2]. Most of the ions are reflected at the angle for specular reflection, i.e., at $\theta_s = 2\theta_i$, since the ions cannot penetrate the topmost atomic plane of the crystal surface when θ_i is less than the critical angle for specular reflection [3].

The inelastic interaction of the specularly reflected ions with the surface takes place along a well-defined trajectory and thus the resulting interaction of the ion is described by the position-dependent interaction probabilities as in the case of the planar channeling [1,2,4]. We have shown that the energy losses of MeV He and H ions, which are specularly reflected from the (100) surfaces of several crystals, are explained by position-dependent stopping powers [5,6]. We have also shown that the charge-state distribution of the specularly reflected MeV He ions is explained with the use of position-dependent electron-loss and -capture probabilities [7,8]. It was shown that the ions scattered at surface steps are deflected at the angles deviated from the angle for specular reflection and that the charge state of the ion does not change after the deflection at the step [8].

Actual crystal surfaces are not atomically flat and have many steps and point defects. At glancing-angle incidence of a beam of ions on the surface, some ions penetrate the surface and reappear from the crystal at the surface steps [9,10]. The energies of these ions are smaller than that of ions reflected from the topmost atomic plane, and, as a result, the energy spectrum of the scattered ions shows a characteristic structure, which depends on the density and distribution of the steps on the surface. The energy spectra of He ions scattered from a SnTe crystal surface have a few well-defined peaks, and the peaks at lower energies have been explained in terms of subsurface planar channeling [3,9]. Thus we can identify the ions reflected from the topmost atomic plane of the surface from their energies since the specularly reflected ions have the least energy loss [3,9,10].

For MeV He ions reflected from the topmost atomic plane of the crystal surface, we observed that the energy loss of the specularly reflected He^{2+} ions is about 10% as large as that of He^+ ions at glancing-angle incidence of He^+ ions on the (100) surface of SnTe [5]. For the ions transmitted through matter, similar differences of energy losses of ions with different charge states have been observed when the charge-state equilibrium of the ions is not attained in the matter: Using thin gas target, Allison *et al.* determined fixed-charge stopping powers for each charge state of H and He ions [11–13]. In channeling conditions, where charge exchange is greatly reduced, it is possible to observe the ions transmitting target without charge exchange [14–16]. Datz *et al.* have observed energy losses that depend on the charge state of the foil transmitted heavy ions after planar channeling in Au single crystals [14]. At transmission through very thin solid foils, it is possible to realize charge-state nonequilibrium of the transmitted ions [17–24]. Cowern and co-workers have measured the charge-state dependence of energy losses of ions passing through very thin carbon foils and derived fixed-charge stopping powers and the energy losses accompanied by electron transfer with the use of a stochastic model [18–21].

In the present paper, we measure the charge state and energy distributions of scattered He ions at glancing angle incidence of MeV He ions on the clean (100) surfaces of SnTe. With the use of the stochastic model of the charge exchange and the energy loss of fast ions in inhomogeneous media, we analyzed our experimental results of the charge state and energy distributions. Position-dependent charge-exchange probabilities of He ions near the surface are derived from the observed distributions.

II. EXPERIMENTAL PROCEDURE

Experimental apparatus was described elsewhere [5–8]. In short, a single crystal of SnTe was prepared by epitaxial growth *in situ* by vacuum evaporation on the cleaved (100) surface of KCl, which had been mounted in a high-precision goniometer in a UHV scattering chamber (base pressure was 3×10^{-10} Torr). A beam of He^+ ions from the 4-MV Van de Graaff accelerator of Kyoto University was collimated by apertures to 0.03 mm$\times$0.03 mm and to a divergence angle less than 0.1 mrad on the target single crystal. The angle of incidence θ_i of the beam to the (100) surface of SnTe was less than 8 mrad, and the ions scattered at an angle θ_s in the plane of scattering, which contains the incident beam and the normal to the surface, were chosen by a movable aperture. The acceptance half angle of the aperture was 0.3 mrad. The ions chosen by the aperture were resolved into their charge states by a magnetic analyzer and the

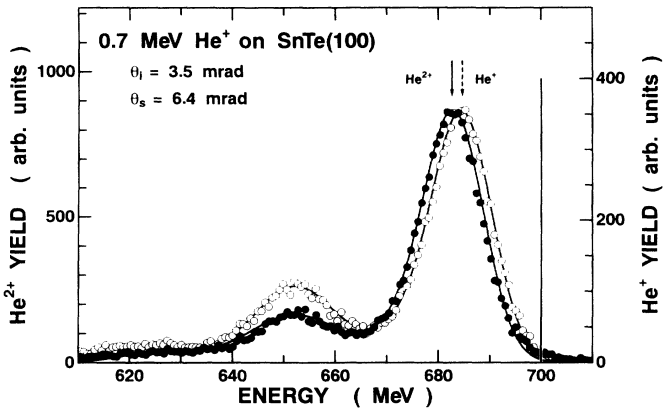

FIG. 1. Energy spectra of scattered He^+ and He^{2+} ions at glancing-angle incidence of 0.7-MeV He^+ ions on the clean SnTe(100) surface. The energy of the incident ions is shown by a vertical line.

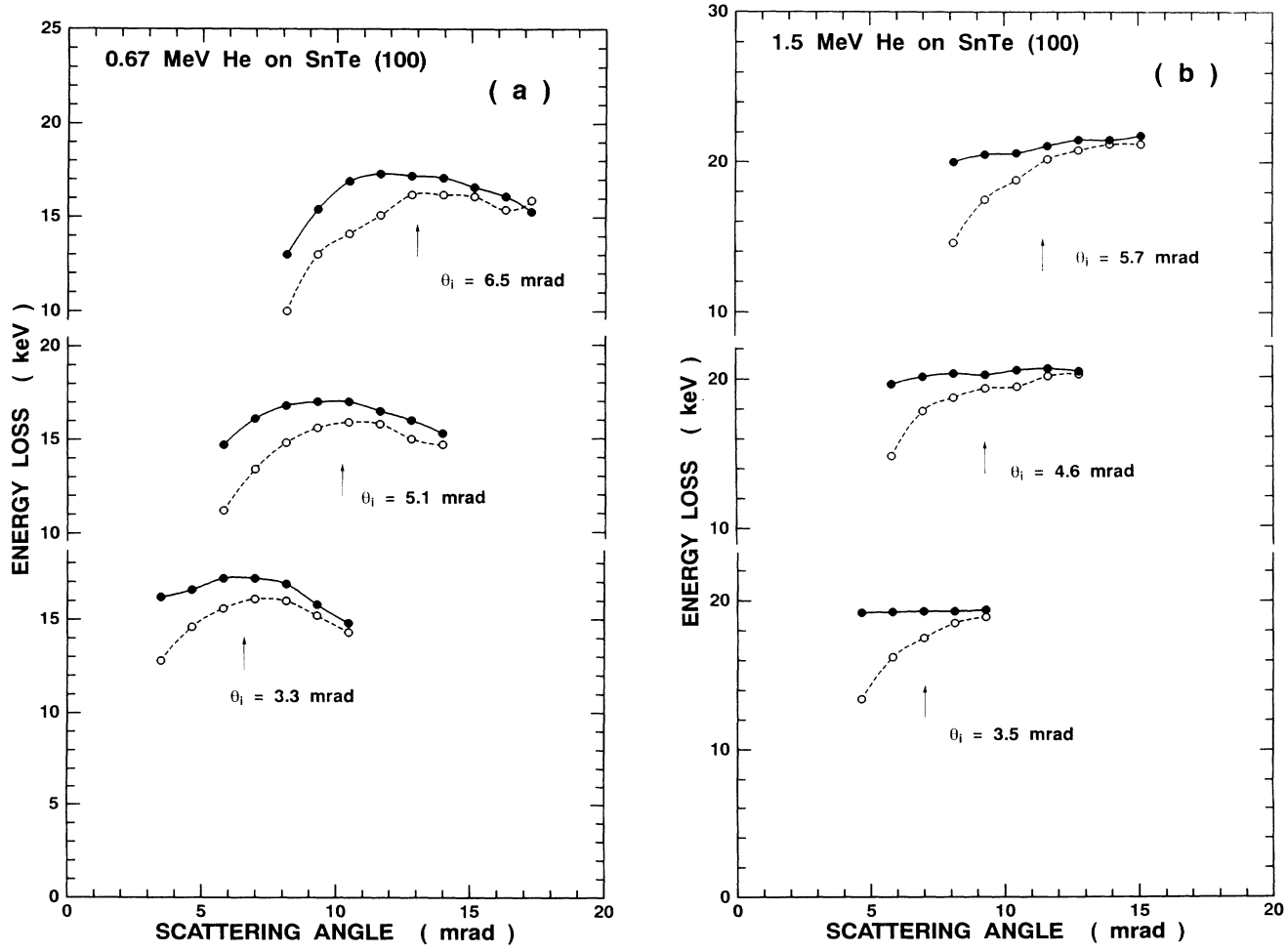

FIG. 2. (a) The energy losses $\Delta E_1(\theta_i;\theta_s)$ (○) and $\Delta E_2(\theta_i;\theta_s)$ (●) of He^+ and He^{2+} ions, for the ions reflected from the (100) surface of SnTe vs the scattering angle, for 0.67-MeV He^+ incident at glancing angles 3.3, 5.1, and 6.5 mrad. The arrows indicate the angles for specular reflection. (b) The energy losses $\Delta E_1(\theta_i;\theta_s)$ (○) and $\Delta E_2(\theta_i;\theta_s)$ (●) of He^+ and He^{2+} ions, for the ions reflected from the (100) surface of SnTe vs the scattering angle, for 1.5-MeV He^+ incident at glancing angles 3.5, 4.6, and 5.7 mrad. The arrows indicate the angles for specular reflection.

energy spectra of the ions with each charge state were measured with a solid-state detector [7,8]. The energy resolution of the solid-state detector was 13 keV for 1-MeV He ions. The aperture and the detector could be rotated ±25 mrad around the direction of the incident beam.

The fractions of He^+ and He^{2+} ions in the scattered beam were measured as follows. To avoid the effect of fluctuations in the incident beam intensity, the magnetic field of the magnetic analyzer was changed periodically so that the He^+ ions and He^{2+} ions reach the detector alternately. The energy spectra of He^+ and He^{2+} ions were registered in two memory groups of a multichannel analyzer, separately. Experimental errors in the observed charge-state fractions could be reduced considerably by this method. Fractions of the neutral ions in the scattered ions were less than 1% for the present experimental conditions, and the energy loss of these ions was not studied.

III. EXPERIMENTAL RESULTS

Energy spectra and charge-state fractions of the scattered ions at glancing angle incidence of 0.67–1.5-MeV He^+ ions on the (100) surface of SnTe were measured. Examples of the energy spectra of the scattered He^+ and He^{2+} ions at glancing-angle incidence of 0.7-MeV He^+ on the clean SnTe(100) surface are shown in Fig. 1, where the energy of the incident ions is shown by a vertical line. The energy spectra of scattered He ions have a few well-defined peaks. The highest-energy peak is due to the He ions specularly reflected from the topmost atomic plane of the surface, while the lower-energy peaks are due to the ions channeled along the (100) planar channels parallel to the surface [3,6,8]. Although the incident ions cannot penetrate atomically flat crystal surface at the angle of incidence smaller than the critical angle for specular reflection, surface penetration occurs at surface steps [3,8,9]. Thus the oscillatory structures of the energy spectra depend on the distribution and density of steps on the reflecting surface plane [3,9].

In the following, we study only the energy loss of the ions reflected from the topmost atomic plane. Since we could not observe the skewness of the highest-energy peak, the peak energy was determined by fitting the peak profile to a Gaussian distribution. The error in the determined peak energy is less than 1% of the width of the distribution, thus the accuracy of the determined mean energy loss is of the order of 0.1 keV. The observed mean energy losses hardly depend on the angle of incidence θ_i, but depend on the scattering angle θ_s and the charge state of the reflected ions. Figures 2(a) and 2(b) show the θ_s dependence of the energy losses of He ions reflected from the topmost atomic plane at glancing-angle incidence of 0.67- and 1.5-MeV He ions, respectively. The energy losses $\Delta E_1(\theta_i;\theta_s)$ of the reflected He^+ ions and $\Delta E_2(\theta_i;\theta_s)$ of the reflected He^{2+} ions are shown by open and filled circles, respectively. They are connected by lines to guide the eyes. The angles of incidence are shown in the figures, and the scattering angles for specular reflection $\theta_s=2\theta_i$ are indicated by arrows. The energy losses of He^{2+} ions are large than those of He^+ ions, and the difference of the energy losses is larger at smaller scattering angles. There is a tendency in the θ_s dependence of the energy loss that the energy losses are smaller at smaller scattering angles ($\theta_s<2\theta_i$). This tendency is more conspicuous in the energy losses of He^+ ions than in those of He^{2+} ions.

The fractions $F_1(\theta_i;\theta_s)$ of the reflected He^+ and $F_2(\theta_i;\theta_s)$ of the reflected He^{2+} ions were measured and have been analyzed previously [7,8]. The fractions depend both on the angle of incidence θ_i and the scattering angle θ_s. The ratios of the observed fractions $F_1(\theta_i;\theta_s)$ and $F_2(\theta_i;\theta_s)$ are reproduced in Fig. 3. The ratios of the fractions of ions scattered at angles smaller than the scattering angle for specular reflection $2\theta_i$ show complicated θ_s dependence, which was attributed to scattering at surface steps [8].

We measured the charge-state fractions of the reflected He ions and the energy losses $\Delta E_1(\theta_i;\theta_s)$ of the reflected He^+ ions and $\Delta E_2(\theta_i;\theta_s)$ of the reflected He^{2+} ions at the incidence of 0.7-MeV He^+ and He^{2+} ions on the (100) surface of SnTe at glancing angle $\theta_i=5$ mrad. The charge-state fractions of the reflected He ions at the He^+ incidence were almost the same as the results of the He^{2+} incidence. The energy losses $\Delta E_i(\theta_i;\theta_s)$ $(i=1,2)$ of the reflected He^+ and He^{2+} ions at the He^+ incidence were similar to the results of the He^{2+} incidence, except that each result of He^{2+} incidence was about 1 keV larger than the result of He^+ incidence.

IV. ANALYSES OF THE RESULTS

A. Charge states and energy losses of specularly reflected ions

Charge state and energy of the ions change along their trajectories of the specular reflection on a surface. To describe the ion trajectory, we define the Cartesian coordinate system, where the x axis is parallel to the surface normal and the scattering plane is in the xz plane. The origin of the coordinates is on the topmost atomic plane of the surface. For the ions at glancing angle incidence on the surface, we now define the probability distribution $f_i(z,E)$ for the ions with charge $+ie$ and energy E on a trajectory $z(x)$. The probability distribution $f_i(z,E)$ satisfies the following relation:

$$f_i(z+\delta z,E)=Q_{ii}(z)\delta z\int_0^\infty [f_i(z,E+\delta E)\omega_i(z;\delta E)\delta z]d(\delta E)$$

$$+\sum_{j\neq i} Q_{ji}(z)\delta z\int_0^\infty [f_j(z,E+U_{ji}+\delta E)\omega_j(z;\delta E)\delta z]d(\delta E)\ , \qquad (1)$$

where

$$Q_{ii}(z)\delta z = 1 - \sum_{j \neq i} Q_{ij}(z)\delta z \ , \tag{2}$$

$\omega_j(z(x);\delta E)$ is the probability (per unit path length and per unit energy) of energy loss δE of He^{j+} ions at the distance x from the surface, $Q_{ij}(z(x))$ is the charge-exchange probability (per unit path length) of the ion from $+ie$ to $+je$ at the distance x from the surface on the trajectory $z(x)$, and U_{ji} is the mean energy loss of the ion due to electron transfer from ionic charge $+je$ to $+ie$. The dependence of $\omega_j(z;\delta E)$ and $Q_{ij}(z)$ on ion energy E is neglected, since the energies of the ions that we are interested in here are almost equal to the energy of incident ions. Expanding $f_i(z+\delta z,E)$, $f_i(z,E+\delta E)$, and $f_j(z,E+U_{ji}+\delta E)$ in Eq. (1) into Taylor series at (z,E) and neglecting the terms containing $(\delta z)^n$ and $(\delta E)^n$ $(n>1)$, we obtain a set of partial differential equations for the evolution of $f_i(z,E)$'s;

$$\frac{\partial f_i(z,E)}{\partial z} = S_i(z(x))\frac{\partial f_i(z,E)}{\partial E} + \sum_{j \neq i} \left\{ Q_{ji}(z) \left[f_j(z,E) + U_{ji}\frac{\partial f_j(z,E)}{\partial E} \right] - Q_{ij}(z) f_i(z,E) \right\} , \tag{3}$$

where $S_i(z(x))$ is the position-dependent stopping power for the ion with charge $+ie$ at a distance x from the surface and is related to $\omega_i(z(x);\delta E)$ as

$$S_i(z(x)) = \int_0^\infty [\delta E\, \omega_i(z(x);\delta E)] d(\delta E) \ . \tag{4}$$

The fraction $F_i(z(x))$ of the ions with charge $+ie$ at $z(x)$ is expressed as

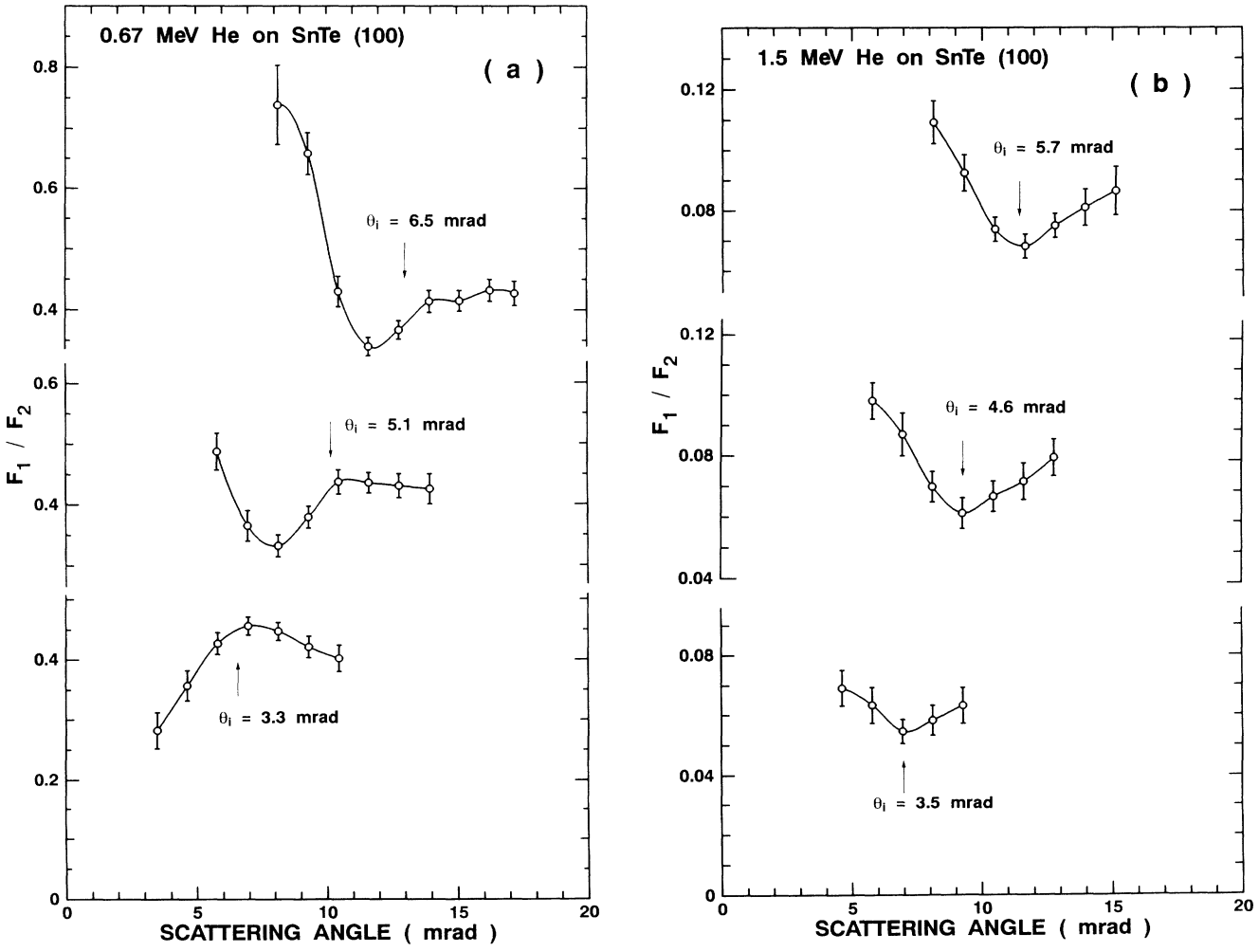

FIG. 3. (a) The ratio of the fraction of He^+ ions $F_1(\theta_i;\theta_s)$ to that of He^{2+} ions $F_2(\theta_i;\theta_s)$ for the ions reflected from the (100) surface of SnTe vs the scattering angle, for 0.67-MeV He^+ incident at glancing-angles 3.3, 5.1, and 6.4 mrad. The arrows indicate the angles for specular reflection. (b) The ratio of the fraction of He^+ ions $F_1(\theta_i;\theta_s)$ to that of He^{2+} ions $F_2(\theta_i;\theta_s)$ for the ions reflected from the (100) surface of SnTe vs the scattering angle, for 1.5-MeV He^+ incident at glancing angles 3.5, 4.6, and 5.7 mrad. The arrows indicate the angles for specular reflection.

$$F_i(z)=\int_0^\infty f_i(z,E)dE \tag{5}$$

and the mean energy $\langle E_i(z)\rangle$ and the mean energy loss $\Delta E_i(z)$ of He^{i+} ions at $z(x)$ are expressed as

$$\langle E_i(z)\rangle=\frac{1}{F_i(z)}\int_0^\infty E f_i(z,E)dE\ , \tag{6}$$

$$\Delta E_i(z)=E_0-\langle E_i(z)\rangle\ , \tag{7}$$

where E_0 is the energy of incident ions. The rate equations for charge state fractions $F_i(z)$ are obtained by integrating Eq. (3) with respect to E as

$$\frac{dF_i(z)}{dz}=\sum_{j\neq 1}[Q_{ji}(z)F_j(z)-Q_{ij}(z)F_i(z)]\ . \tag{8}$$

The evolution of the mean energy loss $\Delta E_i(z)$ of He^{i+} ions along $z(x)$ is obtained by multiplying E to Eq. (3) and integrating with respect to E, and using Eqs. (5)–(7) as

$$\begin{aligned}\frac{d[F_i(z)\Delta E_i(z)]}{dz}&=F_i(z)S_i(z(x))\\&+\sum_{j\neq i}\{Q_{ji}(z)F_j(z)[\Delta E_j(z)+U_{ji}]\\&-Q_{ij}(z)F_i(z)\Delta E_i(z)\}\ .\end{aligned} \tag{9}$$

Equations (8) and (9) are similar to those derived by Cowern and co-workers [18–21].

B. Effect of steps on the ion trajectory

Now we suppose an ion of energy E impinges on an atomically flat surface of a crystal with a small angle θ_i relative to the surface. The equation of motion of the ion is

$$M\frac{d^2x}{dt^2}=-\frac{dV(x)}{dx},\quad M\frac{d^2z}{dt^2}=0\ , \tag{10}$$

where M is the mass of the ion and the energy loss of the ion is neglected. Since the angle of incidence θ_i is small, the potential $V(x)$ in Eq. (10) is approximated to the continuum planar potential of the surface atomic plane as in the case of planar channeling of ion in crystal [1,2]. With the Molière approximation to the Thomas-Fermi screening function, the potential is expressed as

$$V(x)=E\psi_a^2\sum_{i=1}^{3}\frac{\alpha_i}{\beta_i}\exp\left[-\frac{\beta_i x}{a_{\rm TF}}\right]\ , \tag{11}$$

$$\psi_a=\left[\frac{2\pi Z_1Z_2e^2n_pa_{\rm TF}}{E}\right]^{1/2}\ , \tag{11'}$$

where ψ_a is the characteristic angle for planar channeling, Z_1 and Z_2 are the atomic numbers of the ion and the target atom, respectively, e is the elementary charge, n_p is the atomic density of the surface plane, $a_{\rm TF}$ is the Thomas-Fermi screening distance, and α_i and β_i are the parameters in the Molière approximation to the Thomas-Fermi screening function [1,2]. In the following calculations, we neglect the terms $i=1$ and 2 in Eq. (11) because the closest approach of the specularly reflected ions to the surface is larger than $4a_{\rm TF}$ for the present experimental conditions [5]. The error of this approximation is less than 2%. Using this approximation and assuming the apex of the trajectory is at zero on the z axis, the trajectory of the specularly reflected ion can be written as

$$x(z)=\frac{a_{\rm TF}}{\beta_3}\ln\left[\frac{\alpha_3}{\beta_3}\frac{\psi_a^2}{\theta_i^2}\cosh^2\left\{\frac{\beta_3\theta_i z}{2a_{\rm TF}}\right\}\right]\ , \tag{12}$$

The ion is reflected from the surface and scattered at $\theta_s=2\theta_i$ when the angle of incidence θ_i is less than ψ_a. However, actual crystal surface is not an ideal mirror for incident MeV ions, and thus the angular distribution of the reflected ions broadens centered at the angle for specular reflection $\theta_s=2\theta_i$. The broadening is caused by collisions of ions with thermally vibrating atoms (nuclear scattering), electrons (electronic scattering), and surface irregularities. We have shown from a Monte Carlo simulation of angular distributions of specularly reflected ions from a crystal surface that most of the observed broadening comes from the scattering events at surface steps [9,10].

On the other hand, we have shown from atomic force microscopy of the (100) surfaces of epitaxial SnTe crystal that the surface has many small pyramidal hillocks when it is grown at 200 °C at the growth rates larger than about 1 nm/min; and that the step heights are one or two monolayers (3.14 and 6.28 Å) [25]. Possible trajectories of ions scattered at single step at glancing angle incidence on the surface are shown in Fig. 4(a). The ions on the trajectories labeled by A and B which pass over down-

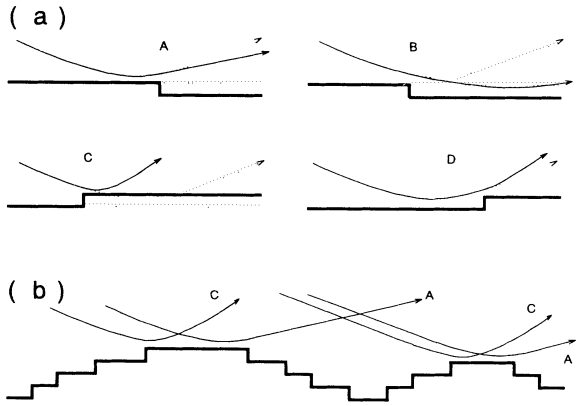

FIG. 4. (a) Possible trajectories of ions scattered at a step at glancing-angle incidence on the surface. The ions on the trajectories labeled by A and B which pass over downsteps are scattered at angles smaller than $\theta_s=2\theta_i$. The ions on the trajectories labeled C and D which pass over upsteps are deflected at angles larger than $2\theta_i$. The dotted lines show specular reflection at a flat surface (dotted lines). (b) The trajectories of scattered ions at the terraced (100) surface of SnTe, where only the trajectories A and C are possible because only the surfaces of top of the small pyramidal hillocks are large enough to reflect the ions.

steps are scattered at angles smaller than $\theta_s = 2\theta_i$. The ions on the trajectors labeled C and D which pass over upsteps are deflected at angles larger than $2\theta_i$. However, only the trajectories A and C are possible on the present surfaces because of the small pyramidal hillocks as shown in Fig. 4(b) [8,10,25].

Now we consider the trajectories of the type A. An ion which has passed over a downstep on its outgoing trajectory is hardly affected by the continuum surface potential as its distance from the surface is larger than the step height (3.14 Å), and thus the trajectory is approximated to a straight line after it passes over the step. The error due to this approximation is less than 1% of θ_s for 0.67-MeV He ions at the angle of incidence 7 mrad. Thus we obtain the following relations:

$$x_s = \frac{a_{\mathrm{TF}}}{\beta_3} \ln\left[\frac{\alpha_3}{\beta_3}\frac{\psi_a^2}{\theta_s(2\theta_i-\theta_s)}\right], \tag{13}$$

$$z_s = \frac{a_{\mathrm{TF}}}{\beta_3\theta_i} \ln\left[\frac{\theta_s^2}{\theta_s(2\theta_i-\theta_s)}\right], \tag{14}$$

where step position z_s, angle of scattering θ_s, and the distance x_s of the ion from the surface at the step position are defined in Fig. 5(a).

C. Role of steps on the charge state and energy loss of reflected ions

We have shown in our previous studies that the position-dependent stopping power $S_i(x)$ and charge-exchange probabilities $Q_{ij}(x)$ are rapidly decreasing functions of x [5–8]. Therefore the charge state and energy of the ions on the type-A trajectories do not change after the ions pass over downsteps, since the distances of the ions on the trajectories from the surfaces are larger than the step height (3.14 Å). Thus the charge state of the ion scattered at an angle θ_s ($<2\theta_i$) is expressed as

$$F_i(\theta_i;\theta_s) = F_i(z_s), \tag{15}$$

where θ_s is related to the position z_s of downstep by Eq. (14). With the use of this relation, we have explained the angular dependence of the charge-state distributions of He ions scattered from the (100) surface of SnTe [8].

We have shown that the energy loss of the ions specularly reflected from the topmost atomic plane on the crystal surface is expressed by integrating the position-dependent stopping power $S(x)$ along its trajectory $z=z(x)$ [5,6]. Since the energy of the ion does not change after it passes over a downstep, the energy of the ion reflected at an angle θ_s ($<2\theta_i$) is equal to that of the ion at the downstep as shown in Fig. 5(b). Thus the energy loss of the ion scattered at θ_s ($<2\theta_i$) is expressed as

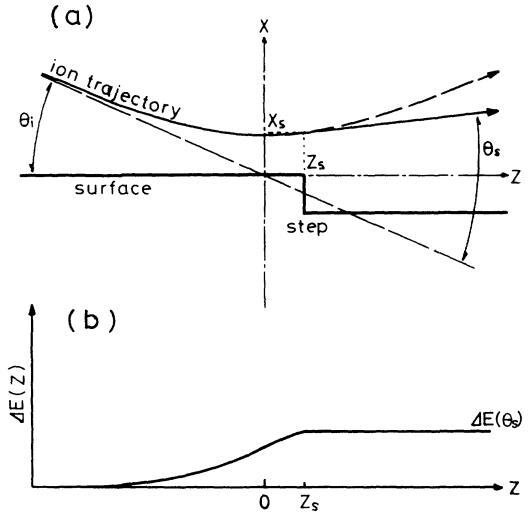

FIG. 5. (a) The type-A trajectory of an ion scattered at a step. The dashed line shows the trajectory of the specularly reflected ion at a flat surface. (b) The evolution of the energy loss of the ion on the trajectory. The closest approach of the ion to the surface is at $z=0$. Step position z_s, scattering angle θ_s, and the distance x_s of the ion from the surface at the step position are defined.

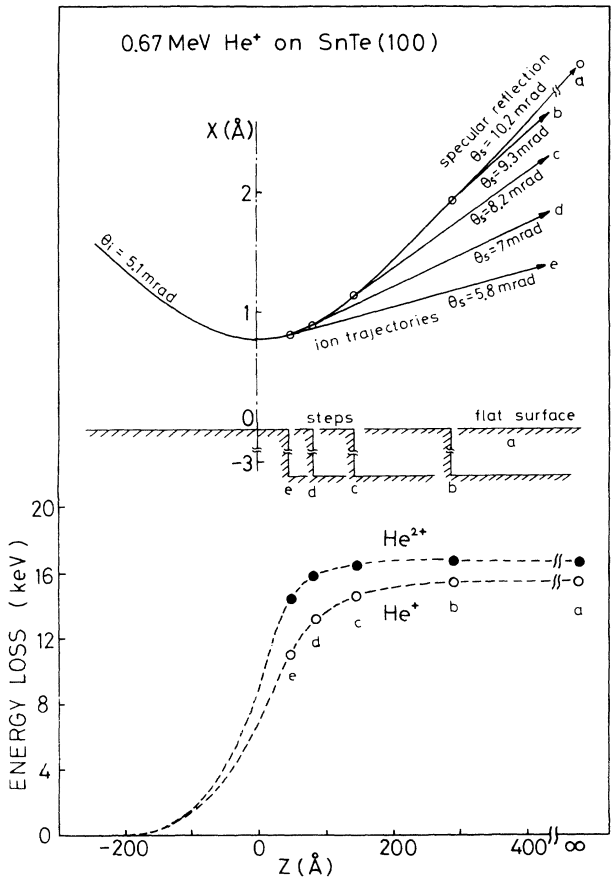

FIG. 6. The evaluations of the energy losses of the He^+ and He^{2+} ions at the position $z=z_s$ along the trajectory of specular reflection for 0.67-meV He^+ ions incident at a glancing angle of $\theta_i=5.1$ mrad, which are derived from the observed energy losses of He^+ and He^{2+} ions scattered at θ_s. Dashed lines are shown as a guide to the eye. The upper part of the figure shows the trajectories of type-A ions scattered at steps, which explain the relation of θ_s and z_s.

$$\Delta E_i(\theta_i;\theta_s)=\Delta E_i(z_s)\ , \tag{16}$$

where θ_s is related to the position z_s of downstep by Eq. (14). Using these relations of Eqs. (14) and (16), we can derive evolution of the energy losses $\Delta E_i(z_s)$ of the He^+ and He^{2+} ions at the position z_s along the trajectories of specular reflection from the observed θ_s dependence of the energy losses $\Delta E_i(\theta_i;\theta_s)$. Figure 6 shows the energy losses of the He^+ and He^{2+} ions at the position $z=z_s$ along the trajectory of specular reflection for 0.67-MeV He^+ ions incident at a glancing angle of $\theta_i=5.1$ mrad, which are derived from the observed energy losses of He^+ and He^{2+} ions scattered at θ_s ($<2\theta_i$) that are shown in Fig. 2(a). Dashed lines are shown to guide the eyes. Inset of the figure shows the trajectories of type-A ions, which explain the relation of θ_s and z_s.

D. Charge states and energy losses of specularly reflected He ions

Now we apply the model in Sec. IV A to the glancing-angle scattering of MeV He ions from the (100) surface of SnTe. Most of the ions reflected from the (100) surface of SnTe are He^+ and He^{2+}, and the fraction of He^0 ions is less than 1% at glancing-angle scattering of MeV He ions from the (100) surface of SnTe. We therefore consider only the fractions of He^+ and He^{2+}, i.e., $F_1(z)$ and $F_2(z)$. The rate equations for the charge-state fractions, Eq. (8), reduce to two simultaneous equations and are solved when the initial fractions are given. When the fraction of He^+ ions in the incident He ions is $F_1^{\rm in}$ at $x=\infty, z=-\infty$, and thus $F_2^{\rm in}=1-F_1^{\rm in}$, Eq. (8) for $F_1(z)$ is integrated

$$F_1(z(x))=\int_{-\infty}^{z}Q_{21}(x')\exp\left\{-\int_{z'}^{z}[Q_{12}(x'')+Q_{21}(x'')]dz''\right\}dz'+F_1^{\rm in}\exp\left\{-\int_{-\infty}^{z}[Q_{12}(x')+Q_{21}(x')]dz'\right\} \tag{17}$$

and

$$F_2(z(x))=1-F_1(z(x))\ , \tag{18}$$

where the integrations in Eq. (17) are performed along the ion trajectory $z(x)$.

For convenience of the following discussion, we define the equilibrium charge-state fractions of He ions which are attained for the ions moving parallel to the surface at the distance x. The equilibrium charge-state fractions $F_i^{\rm eq}(x)$ of the ions are related to the charge-exchange probabilities

$$F_i^{\rm eq}(x)=\frac{Q_{ji}(x)}{Q_{12}(x)+Q_{21}(x)}\quad (j\neq i)\ , \tag{19}$$

where i and j are 1 and 2.

Integrating Eq. (9) along the ion trajectory with the initial condition that $\Delta E_i(-\infty)=0$, we obtain two relations for the energy losses $\Delta E_1(z)$ and $\Delta E_2(z)$ of He ions at $z(x)$ on the trajectory of specular reflection; the mean value $\Delta E_m(z)$ of the energy losses on the charge states of the He ions as

$$\begin{aligned}\Delta E_m(z)&=F_1(z)\Delta E_1(z)+F_2(z)\Delta E_2(z)\\&=\int_{-\infty}^{z}\{[S_1(x')+Q_{12}(x')U_{12}]F_1(z')\\&\qquad+[S_2(x')+Q_{21}(x')U_{21}]F_2(z')\}dz'\ ,\end{aligned} \tag{20}$$

and the difference $\Delta E_{21}(z)$ of the energy losses of He^{2+} and He^+ as

$$\Delta E_{21}(z)=\Delta E_2(z)-\Delta E_1(z)=\int_{-\infty}^{z}\left\{\left[S_2(x')+Q_{12}(x')U_{12}\frac{F_1(z')}{F_2(z')}\right]-\left[S_1(x')+Q_{21}(x')U_{21}\frac{F_2(z')}{F_1(z')}\right]\right\}\times\exp\left[-\int_{z'}^{z}\left[Q_{21}(x'')\frac{F_2(z'')}{F_1(z'')}+Q_{12}(x'')\frac{F_1(z'')}{F_2(z'')}\right]dz''\right]dz'\ . \tag{21}$$

From these relations, $\Delta E_1(z)$ is derived:

$$\begin{aligned}\Delta E_1(z)=\int_{-\infty}^{z}&\left[[S_1(x')F_1(z')+Q_{21}(x')U_{21}F_2(z')]\left[1+\frac{F_2(z')}{F_1(z)}\exp\left\{-\int_{z'}^{z}[Q_{21}(x'')+Q_{12}(x'')]dz''\right\}\right]\right.\\&\left.+[S_2(x')F_2(z')+Q_{12}(x')U_{12}F_1(z')]\left[1-\frac{F_1(z')}{F_1(z)}\exp\left\{-\int_{z'}^{z}[Q_{21}(x'')+Q_{12}(x'')]dz''\right\}\right]\right]dz'\ .\end{aligned} \tag{22}$$

We can obtain a similar equation for $\Delta E_2(z)$. Equation (22) is rewritten in a simpler form,

$$\Delta E_i(z)=\frac{1}{F_i(z)}\int_{-\infty}^{z}[M_i(z')P_{ii}(z',z)+M_j(z')P_{ji}(z',z)]dz'(i\neq j)\ , \tag{23}$$

$$M_i(z')=S_i(x')F_i(z')+Q_{ji}(x')U_{ji}F_j(z')\ , \tag{24}$$

$$P_{ji}(z',z)=\int_{z'}^{z}\left[Q_{ji}(x'')\exp\left\{-\int_{z''}^{z}[Q_{21}(x''')+Q_{12}(x''')]dz'''\right\}\right]dz'' , \tag{25}$$

$$P_{ii}(z',z)=1-P_{ij}(z',z) . \tag{26}$$

$M_j(z')dz'$ shows the energy-loss moment of He^{j+} in the interval $(z',z'+dz')$ and is the sum of the energy-loss moment due to the stopping $S_j(x')$ of He^{j+} ions without charge changing and that due to the energy loss U_{ij} in the charge-exchange collision in which the He^{i+} ion changes into the He^{j+} ion. $P_{ji}(z',z)$ shows the fraction of the He ions in the charge state i at the position $z(x)$ that were in the charge state j at the position $z'(x')$. They satisfy the following relations:

$$F_i(z)=P_{1i}(z',z)F_1(z')+P_{2i}(z',z)F_2(z') , \tag{27}$$

$$P_{i1}(z',z)+P_{i2}(z',z)=1 . \tag{28}$$

E. Derivation of charge-exchange probabilities

We write down the position-dependent stopping power for specularly reflected ion with unit point charge $+e$ by $S_p(x)$. From the analogy of the effective-ion-charge model for the stopping power of bulk material [26–28] we express the fixed-charge position-dependent stopping power as

$$S_j(x)=q_j^2S_p(x) , \tag{29}$$

where q_je is the effective charge of the He^{j+} ion. Substituting Eq. (29) into Eqs. (20) and (21), we obtain the mean value $\Delta E_m(z)$ of the energy losses of He^{2+} and He^{+} ions as

$$\begin{aligned}\Delta E_m(z)=\int_{-\infty}^{z}\{&[F_1(z')q_1^2+F_2(z')q_2^2]S_p(x')\\&+Q_{12}(x')U_{12}F_1(z')\\&+Q_{21}(x')U_{21}F_2(z')\}dz'\end{aligned} \tag{30}$$

and the difference $\Delta E_{21}(z)$ of the energy losses of He^{2+} and He^{+} as

$$\Delta E_{21}(z)=\frac{1}{F_1(z)F_2(z)}\int_{-\infty}^{z}\left[\{(q_2^2-q_1^2)S_p(x')F_1(z')F_2(z')+Q_{12}(x')U_{12}F_1(z')^2-Q_{21}(x')U_{21}F_2(z')^2\}\times\exp\left\{-\int_{z'}^{z}[Q_{21}(x'')+Q_{12}(x'')]dz''\right\}\right]dz' . \tag{31}$$

From Eqs. (30), (31), and (8), the charge-exchange probabilities $Q_{ji}(x)$ are derived as follows:

$$\begin{aligned}Q_{ji}(x)=F_i(z)&\left\{\frac{d[q_j^2\Delta E_i(z)-q_i^2\Delta E_j(z)]}{dz}+\frac{q_i^2[\Delta E_{ij}(z)+U_{ij}]}{F_j(z)}\frac{dF_j(z)}{dz}\right\}\\&\times\{[q_1^2F_1(z)+q_2^2F_2(z)]\Delta E_{ji}(z)+q_j^2U_{ji}F_j(z)-q_i^2U_{ij}F_i(z)\}^{-1}\end{aligned} \tag{32}$$

where $z=z(x)$ and $i\neq j$. This shows that we can determine the position-dependent charge-exchange probabilities $Q_{ji}(x)$ from the observed energy losses $\Delta E_i(z)$ and observed charge-state fractions $F_i(z)$, provided that we know the q_je and U_{ij}. It can be seem from Eq. (32) that the charge-exchange probabilities are small when the difference $\Delta E_{ij}(z)$ of the energy losses is large.

From the kinematics of collision process [29], the energy loss U_{21} of the He^{2+} ion at electron capture is

$$U_{21}=B_T-B_P , \tag{33}$$

where B_T and B_P are the (positive) binding energies of the electron in the target shown atom and the He^{+} ion, respectively. Taking account of the velocity matching, the He^{2+} ion captures an electron mainly from the $4s$ state of Sn and Te atoms in the present energy region. The binding energies of the $4s$ electrons of Sn and Te atoms are 133 and 162 eV for Sn and Te, respectively [30]. Thus we obtain $U_{21}\sim 0.09$ keV. For the electron-loss process of He^{+}, we assume that the velocity of the lost electron relative to the ion is small. Thus the energy loss U_{12} of the He^{+} ion at electron loss is expressed as

$$U_{12}\sim\tfrac{1}{2}mV^2 , \tag{34}$$

where V is the laboratory-frame velocity of the ion and m is electron mass. U_{12} is 0.09 and 0.2 keV for 0.67- and 1.5-MeV He ions, respectively.

Because the He^{2+} ion has no bound electron, its effective charge is $+2e$, i.e., $q_2=2$, while the effective charge of the He^{+} ion depends on the He^{+} velocity. Now, for convenience in the following analysis, we assume $q_1=1$. We will discuss this assumption in Sec. V.

Now substituting the values of q_1, q_2, U_{12}, and U_{21} into Eq. (32), and using Eqs. (15) and (16) to derive $F_i(z)$ and $\Delta E_i(z)$ from the experimental data, and using the following relation derived from Eq. (14):

$$d\theta_s=\frac{\beta_3}{2a_{\mathrm{TF}}}\theta_s(2\theta_i-\theta_s)dz , \tag{35}$$

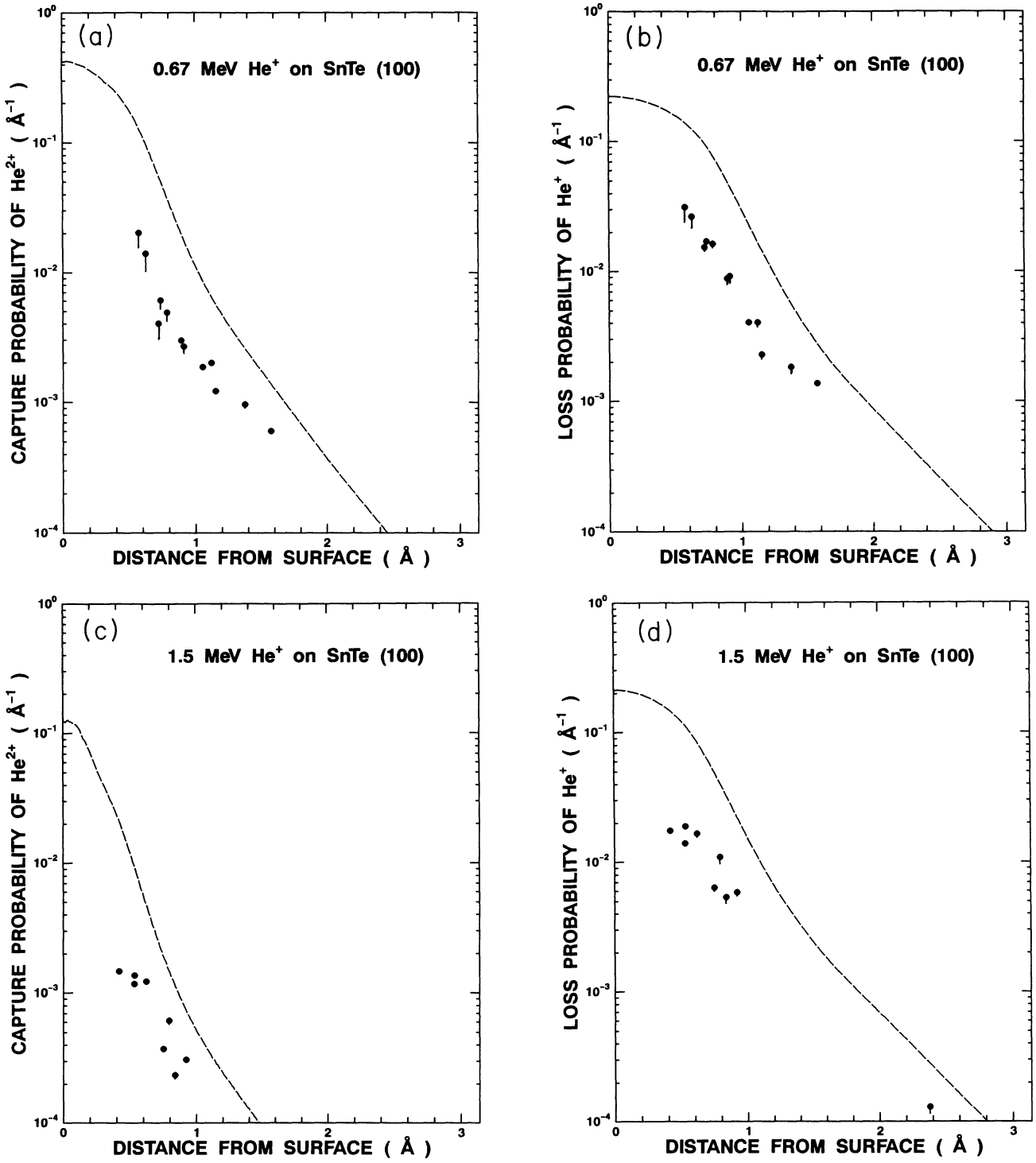

FIG. 7. (a) Experimentally derived position-dependent electron-capture probabilities, $Q_{21}(x)$ for 0.67-MeV He ions at the (100) surface of SnTe. For comparison, the calculated position-dependent charge-exchange probabilities are shown by dashed lines, which probabilities are calculated with the use of the Bohr and the Bohr-Lindhard models. (b) Experimentally derived position-dependent electron-loss probabilities, $Q_{12}(x)$ for 0.67-MeV He ions at the (100) surface of SnTe. For comparison, the calculated position-dependent charge-exchange probabilities are shown by dashed lines, which probabilities are calculated with the use of the Bohr and the Bohr-Lindhard models. (c) Experimentally derived position-dependent electron-capture probabilities, $Q_{21}(x)$ for 1.5-MeV He ions at the (100) surface of SnTe. For comparison, the calculated position-dependent charge-exchange probabilities are shown by dashed lines, which probabilities are calculated with the use of the Bohr and the Bohr-Lindhard models. (d) Experimentally derived position-dependent electron-loss probabilities, $Q_{12}(x)$ for 1.5-MeV He ions at the (100) surface of SnTe. For comparison, the calculated position-dependent charge-exchange probabilities are shown by dashed lines, which probabilities are calculated with the use of the Bohr and the Bohr-Lindhard models.

we obtain the position-dependent charge-exchange probabilities $Q_{12}(x)$ and $Q_{21}(x)$.

Figure 7 shows the obtained charge exchange probabilities for 0.67- and 1.5-MeV He ions at the (100) surface of SnTe. The obtained charge-exchange probabilities in Fig. 7 decrease with the increasing distance of the ion from the surface. For comparison, the calculated charge-exchange probabilities are shown by dashed lines in Fig. 7. They were calculated by averaging the charge-exchange cross sections for He-Sn and He-Te collisions over the surface plane. The cross sections were calculated with the Bohr and the Bohr-Lindhard models [31,32]. Agreement of the calculated and observed probabilities is poor, and the calculated probabilities are almost four times as large as the observed ones, a more elaborate theory is needed. But the ratios of the $Q_{12}(x)/Q_{21}(x)$ are almost the same, and the equilibrium charge-state fractions F_i^{eq} given by Eq. (19) for these two sets of probabilities agree as shown in Fig. 8. Due to this agreement, the observed charge-state distributions were well explained in terms of the Bohr and the Bohr-Lindhard models [8].

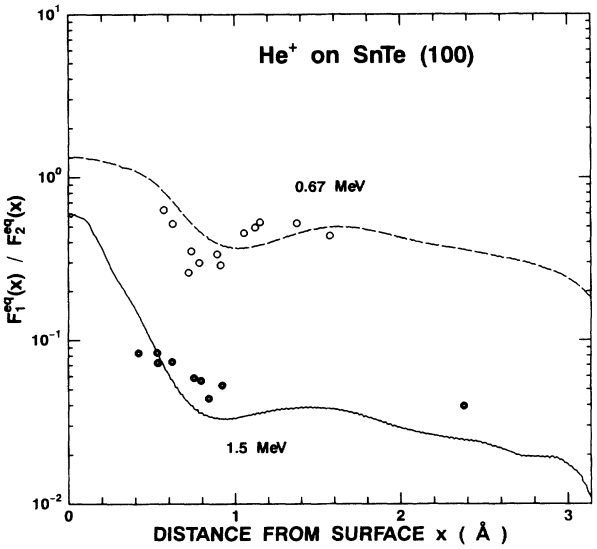

FIG. 8. Ratios of equilibrium charge state fractions $F_1^{eq}(x)$ and $F_2^{eq}(x)$ of 0.67- and 1.5-MeV He ions near the (100) surface of SnTe. Circles are calculated from the charge-exchange probabilities derived from the present analysis, while the dashed lines are calculated from the theoretical probabilities.

V. DISCUSSION

The stochastic model for the probability distribution $f_i(z,E)$ has originally been described by Winterbon [33] and developed by Cowern and co-workers at foil transmission of fast ions [18–21]. For a better understanding of the physical meaning of Eq. (23) for the energy loss $\Delta E_i(z)$, we consider two extreme cases. The first is the case where the charge-exchange does not occur during specular reflection. In this case, both $Q_{12}(z)$ and $Q_{21}(z)$ are zero, and the $P_{ii}(z',z)$'s defined by Eq. (25) are

$$P_{ii}(z',z)=1, \quad P_{ij}(z',z)=0 \quad (i\neq j) . \tag{36}$$

Thus the energy losses are written down simply as

$$\Delta E_i(z(x))=\int_{-\infty}^{z} q_i^2 S_p(z'(x'))dz' . \tag{37}$$

The energy loss of He^{j+} ions is proportional to q_j^2.

The second is the case where the charge-exchange occurs so frequently that the ions are in the charge-state equilibrium at any point on the trajectory $z(x)$, where the fractions are given by Eq. (19). In this case, it is seen from Eq. (25) that

$$P_{ji}(z',z)=F_i(z(x))=F_i^{eq}(z(x)) . \tag{38}$$

The energy losses of He^+ and He^{2+} ions are the same and are given as

$$\Delta E_1(z)=\Delta E_2(z)=\Delta E_m(z)=\int_{-\infty}^{z}\{[F_1^{eq}(z')q_1^2+F_2^{eq}(z')q_2^2]S_p(x') + F_1^{eq}(z')F_2^{eq}(z')(U_{12}+U_{21})[Q_{12}(z')+Q_{21}(z')]\}dz' . \tag{39}$$

The actual situations are intermediate between the two extreme cases above and can be solved numerically.

As can be seen from Eq. (32) the position-dependent charge-exchange probabilities can be derived from only the energy and charge-state distribution of the ions scattered from the surface regardless of the initial charge state of incident He ions. We performed the experiment of He^{2+} incidence at 0.7-MeV He. The experimental results were similar to the results of He^+ incidence, and the charge-exchange probabilities derived from the results of He^{2+} incidence were almost the same as those derived from the results of He^+ incidence.

In deriving the charge-exchange probabilities from Eq. (32), we assumed that the effective charge $q_1 e$ of the He^+ ion is e. This is based on the following consideration: In the cases of foil transmission of the fast He^+ ion through foils, the effective charge of He^+ is generally larger than $+e$, except the low-velocity He^+ ions where the screening effect by a bound electron in He^+ is strong. As the velocity increases, the effective charge becomes larger because the ions are subjected to close collisions with target electrons [34]. On the other hand, at glancing-angle scattering of fast ions from a surface, the impact parameter of ion-atom collisions is larger than the Thomas-Fermi screening distance of the collisions. Thus the contribution of close collisions to the stopping of the ions is smaller than that of the ion in solid. The nuclear charge of He^+ is well screened by the bound electron for distant collisions. A similar situation is realized in channeling. From the observed stopping powers for heavy ions in

Au(111) channels, Datz *et al.* have shown that the screening per electron of the ion, which is defined as (Z_1-q_{eff})/(number of bound electrons), was about 0.9 [14]. This shows that the nuclear charge is well screened by the bound electrons for channeling ions.

In order to see the effect of the effective charge $q_1 e$ of the He^+ ion on the derived charge-exchange probabilities, we calculated the charge-exchange probabilities with $q_1=1-1.2$. The calculated results are shown by solid bars in Fig. 7. Although the calculated charge-exchange probabilities with larger q_1 are slightly smaller, the difference is relatively small.

In deriving the charge-exchange probabilities with Eq. (32), we needed U_{ij}. In order to show the effect of the U_{ij} on the derived charge-exchange probabilities, we calculated the charge-exchange probabilities with the use of $U_{ij}=0$. The calculated results are slightly larger, but in the filled circle in Fig. 7. It can be seen that the effect of U_{ij} on the derived charge-exchange probabilities is very small.

VI. CONCLUSION

We measured charge-state fractions and energy losses of He^+ and He^{2+} ions scattered from the (100) surface of a SnTe crystal at glancing angles of incidence for MeV He^+ ions. Based on the model that the deflection of ions from the trajectory of specular reflection occurs at surface step, the observed charge state and energy losses of He ions were related to those of ions just above the step. For the interpretation of the experimental results, a stochastic model was formulated to describe the change in the charge-state fraction and energy loss of ions traveling along a surface reflecting trajectory. It was shown from the model that the difference of energy losses of scattered He^+ and He^{2+} ions is useful to derive the position-dependent charge-exchange probabilities of scattered He ions. With the use of the relations of charge-state distributions and energy losses of scattered He ions derived from the stochastic model, the charge-exchange probabilities of MeV He ions at the (100) surface of SnTe were derived, which depend on the distance from the surface plane.

ACKNOWLEDGMENTS

We are grateful to K. Yoshida and K. Norisawa and other staff members of the Department of Nuclear Engineering of Kyoto University for the availability of the 4MV Van de Graaff accelerator. The work was partly supported by a Grant-in-Aid for Scientific Research from the Ministry of Education, Science and Culture.

[1] J. Lindhard, K. Dan. Vidensk. Selsk. Mat. Fys. Medd. **34**, No. 14 (1965).
[2] D. S. Gemmell, Rev. Mod. Phys. **46**, 129 (1974).
[3] K. Kimura, M. Hasegawa, Y. Fujii, M. Suzuki, Y. Susuki, and M. Mannami, Nucl. Instrum. Methods B **33**, 358 (1988).
[4] M. T. Robinson, Phys. Rev. B **4**, 1461 (1971).
[5] K. Kimura, M. Hasegawa, and M. Mannami, Phys. Rev. B **36**, 7 (1987).
[6] Y. Fujii, S. Fujiwara, K. Narumi, K. Kimura, and M. Mannami, Surf. Sci. **277**, 164 (1992).
[7] K. Kimura, Y. Fujii, M. Hasegawa, Y. Susuki, and M. Mannami, Phys. Rev. B **38**, 1052 (1988).
[8] Y. Fujii, S. Fujiwara, K. Kimura, and M. Mannami, Nucl. Instrum. Methods B **58**, 18 (1991).
[9] M. Mannami, Y. Fujii, and K. Kimura, Surf. Sci. **204**, 213 (1989).
[10] Y. Fujii, K. Kimura, M. Hasegawa, M. Suzuki, Y. Susuki, and M. Mannami, Nucl. Instrum. Methods B **33**, 405 (1988).
[11] S. K. Allison, J. Cuevas, and M. García-Munoz, Phys. Rev. **127**, 792 (1962).
[12] M. N. Huberman, Phys. Rev. **127**, 799 (1962).
[13] J. Cuevas, M. García-Munoz, P. Torres, and S. K. Allison, Phys. Rev. **135**, A335 (1964).
[14] S. Datz, J. Gomez del Campo, P. F. Dittner, P. D. Miller, and J. A. Biggerstaff, Phys. Rev. Lett. **38**, 1145 (1977).
[15] J. A. Golovchenko, A. N. Goland, J. S. Rosner, C. E. Thorn, H. E. Wegner, H. Knudsen, and C. D. Moak, Phys. Rev. B **23**, 957 (1981).
[16] J. A. Golovchenko, D. E. Cox, and A. N. Goland, Phys. Rev. B **26**, 2335 (1982).
[17] L. F. Pender and H. J. Hay, Nucl. Instrum. Methods B **4**, 72 (1984).
[18] N. E. B. Cowern, P. M. Read, C. J. Sofield, L. B. Bridwell, G. Huxtable, M. Miller, and M. W. Lucas, Nucl. Instrum. Methods B **2**, 112 (1984).
[19] N. E. B. Cowern, P. M. Read, C. J. Sofield, L. B. Bridwell, and M. W. Lucas, Phys. Rev. A **30**, 1682 (1984).
[20] N. E. B. Cowern, P. M. Read, and C. J. Sofield, Nucl. Instrum. Methods B **12**, 43 (1985).
[21] L. B. Bridwell, N. E. B. Cowern, P. M. Read, and C. J. Sofield, Nucl. Instrum. Methods B **13**, 123 (1986).
[22] E. M. Bernstein, Nucl. Instrum. Methods B **40/41**, 205 (1989).
[23] H. Ogawa, I. Katayama, H. Ikegami, Y. Haruyama, A. Aoki, M. Tosaki, F. Fukuzawa, K. Yoshida, I. Sugai, and T. Kaneko, Phys. Rev. B **43**, 11 370 (1991).
[24] H. Ogawa, I. Katayama, H. Ikegami, Y. Haruyama, A. Aoki, M. Tosaki, F. Fukuzawa, K. Yoshida, and I. Sugai, Phys. Lett. A **160**, 77 (1991).
[25] K. Narumi, Y. Fujii, K. Kimura, M. Mannami, and H. Hara, Surf. Sci. (to be published).
[26] N. Bohr, Phys. Rev. **58**, 654 (1940); **59**, 270 (1941).
[27] W. E. Lamb, Phys. Rev. **58**, 696 (1940).
[28] W. Brandt, *Atomic Collisions in Solids* (Plenum, New York, 1973), Vol. 1, p. 261.
[29] L. B. Bridwell, H. J. Hay, L. F. Pender, C. J. Sofield, and P. B. Treacy, Aust. J. Phys. **40**, 125 (1987).
[30] H. Herman and S. Skillman, *Atomic Structure Calculations* (Prentice-Hall, Englewood Cliffs, NJ, 1963).
[31] N. Bohr, K. Dan. Vidensk. Selsk. Mat. Fys. Medd. **18**, No. 8 (1948).
[32] N. Bohr and J. Lindhard, K. Dan. Vidensk. Selsk. Mat. Fys. Medd. **28**, No. 7 (1954).
[33] K. B. Winterbon, Nucl. Instrum. Methods **144**, 311 (1977).
[34] T. Kaneko, Nucl. Instrum. Methods B **67**, 73 (1992).